Available online at www.sciencedirect.com
SCIENCE DIRECT®
Journal of Power Sources 128 (2004) 152–164
JOURNAL OF POWER SOURCES
www.elsevier.com/locate/jpowsour

Improvement of electricity generating performance and life expectancy of MCFC stack by applying Li/Na carbonate electrolyte Test results and analysis of 0.44 m^2/10 kW- and 1.03 m^2/10 kW-class stack

Fumihiko Yoshiba [a,*], Hiroshi Morita [a], Masahiro Yoshikawa [a], Yoshihiro Mugikura [a], Yoshiyuki Izaki [a], Takao Watanabe [a], Mineo Komoda [b], Yuji Masuda [c], Nobuyuki Zaima [c]

[a] *Chemical Energy Engineering Department, Yokosuka Research Laboratory, Central Research Institute of Electric Power Industry, 2-6-1 Nagasaka, Yokosuka 240-0196, Japan*
[b] *Chubu Electric Power Co., Inc., Japan*
[c] *Ishikawajima-Harima Heavy Industries Co. Ltd., Japan*

Received 20 August 2003; received in revised form 26 September 2003; accepted 15 October 2003

Abstract

Following the development of a 10 kW-class MCFC stack with a reactive area of 0.44 and 1.03 m^2, which applies a Li/Na carbonate electrolyte and a press stamping separator, many tests have now been carried out. In the installation tests, the observed cell voltages of the 0.44 m^2/10 kW-class stack agreed with the voltage predicted from the test results of the 100 cm^2 bench scale cell. This agreement proves that the installing procedure of the bench scale cell can be applied to the 0.44 m^2/10 kW-class stacks. The temperature distribution analysis model applied to the 100 kW-class stack was modified to calculate the temperature distribution of the 0.44 m^2/10 kW-class stack. Taking the heat loss and the heat transfer effect of the stack holder into account, the calculated temperature was close to the measured temperature; this result proves that the modification was adequate for the temperature analysis model. In the high current density operating tests on the 0.44 m^2/10 kW-class stack, an electrical power density of 2.46 kW/m^2 was recorded at an operating current density of 3000 A/m^2. In the endurance test on the 0.44 m^2/10 kW-class stack, however, unexpected Ni shortening occurred during the operating period 2500–4500 h, which had been caused by a defective formation of the electrolyte matrix. The shortening seems to have been caused by the crack, which appeared in the electrolyte matrix. The voltage degradation rate of the 0.44 m^2/10 kW-class stack was 0.52% over 1000 h, which proves that the matrix was inadequate for a long life expectancy of the MCFC stack. A final endurance test was carried out on the 1.03 m^2/10 kW-class stack, of which the matrix had been revised. The fuel utilisation and the leakage of anode gas never changed during the 10,000 h operating test. This result suggests that no shortening occurred during the 10,000 h endurance test. The cell voltage degradation rate was around 0.2–0.3% over 1000 h in the 1.03 m^2/10 kW-class stack. According to a comparison of the stack electricity generating performance of the 0.44 m^2 and the 1.03 m^2/10 kW-class stack under the same operating conditions, the performance of the 1.03 m^2 stack was lower at the beginning of the endurance test, however, its performance exceeded the performance of the 0.44 m^2/10 kW-class stack during the 10,000 h operating test. By carrying out the high current density operating test and the 10,000-hour endurance test using commercial sized 10 kW-class stacks, the stability of the MCFC stack with a Li/Na carbonate electrolyte and a press stamping separator has been proven.

Keywords: Molten carbonate fuel cell; Li/Na carbonate electrolyte; 10 kW-class stack; Life endurance test; Temperature analysis

1. Introduction

Because their output voltage is high [1], it is to be expected that molten carbonate fuel cells (MCFCs) will be used as high efficiency power generation systems. The aim is to introduce this technology into centralised power stations or distributed power plants. The author's research group has been conducting operating tests on bench scale cells and 10 kW-class MCFC stacks since FY1987 [2,3]. The experience gained during the operation of bench scale cells and 10 kW-class stacks has been applied to operating tests on 100 kW-class stacks, and the electricity generating performance of the stack has been approved [4]. The configuration of the 100 kW-class stack has been applied to a 1 MW

* Corresponding author. Tel.: +81-46-856-2121; fax: +81-46-856-3346.
E-mail address: yoshiba@criepi.denken.or.jp (F. Yoshiba).

0378-7753/$ – see front matter © 2003 Elsevier B.V. All rights reserved.
doi:10.1016/j.jpowsour.2003.10.011

Nomenclature

A_a	frequency factor of anode resistance
A_{c_1}, A_{c_2}, A_{c_3}	frequency factor of cathode resistance
A_{ir}	frequency factor of internal resistance
E	open circuit voltage of individual cell
E^0	standard electromotive force
F	Faraday's constant
ΔH_a	activation energy of anode resistance
ΔH_{c_1}, ΔH_{c_2}, ΔH_{c_3}	activation energy of cathode resistance
ΔH_{ir}	activation energy of internal resistance
j	current density
m_i	molar fraction of species i
p_i	partial pressure of species i
R	universal gas constant
R_a	anode polarisation
R_c	cathode polarisation
R_{ir}	internal resistance
T	temperature
V	voltage of individual cell
Subscript	
a and c	anode and cathode, respectively

pilot plant operation, and the plant has succeeded in connecting to the electricity distribution network [5]. In these tested cells and stacks, a Li_2/K_2CO_3 carbonate melt was applied as the electrolyte, and corrugated plate was appointed as their separators. The output cell voltage of the stacks was around 800 mV at an operating current density of 1500 A/m^2 and, therefore, satisfied the target voltage of national projects in Japan. The degradation rate of the stacks' cell voltage, however, did not meet the target of national projects. For future prospects regarding energy efficiency and the life expectancy of MCFC power plants, the output voltage of the stacks is insufficient to make a market entry. In this study, we have focused on the electrolyte carbonate composition and the shape of the separator to achieve a higher electricity generating performance and a longer life expectancy of the stacks.

Janz and Saegusa [6] estimated the viscosities of Li_2CO_3, Na_2CO_3 and K_2CO_3 as a function of the temperature, which they expressed in the Arrhenius' equation based on the experimental and theoretical method. Broers and Van Ballegoy [7] discussed the stability of Al_2O_3 alumina in the carbonate melt mixture of Li_2CO_3, Na_2CO_3 and K_2CO_3. Ang and Sammells [8] compared the ionic conductivities of Li/Na/K, Li/K and Li/Na carbonate melts at 600 °C and also the life expectancy of each carbonate mixture. In their study, the highest ionic conductivity and the lowest vapourability have been predicted for the Li/Na carbonate mixture. Tanimoto et al. [9] carried out the operating test on a laboratory-scale cell and compared the cell performance with the Li, K, Na carbonate having added Ca, Sr, Ba. According to these investigations and a further survey regarding the material characteristics of the electrolyte melt, the Li/Na carbonate electrolyte has a greater possibility of achieving a higher performance than the Li/K carbonate electrolyte due to its higher ion conductivity [10–12]. Concerning greater durability, the Li/Na carbonate electrolyte has an advantage over the Li/K carbonate electrolyte since the solubility of the NiO cathode in the Li/Na carbonate is lower than the solubility in the Li/K carbonate. Ota et al. [13] measured the solubility of the NiO cathode in the Li/K and Li/Na carbonate, and a greater stability of the NiO was observed in the Li/Na carbonate than in the Li/K carbonate. A further disadvantage of the Li/Na carbonate melt is that the solubility of oxygen in the Li/Na carbonate melt is lower than in Li/K, and it is this phenomenon which causes the larger cathode polarisation in the Li/Na carbonate stacks. This disadvantage, however, is eliminated when the stack is operated in pressurised conditions since the solubility of cathode oxygen is greater in high-pressure environments. We can therefore state that the disadvantage of the solubility is less severe than the advantage of high ion conductivity.

A corrugated type separator is adequate to diffuse fuel and oxidant gas in the gas channel of the reactive area. However, the separator's contact area with the electrolyte is large, which again causes electrolyte loss. Moreover, the fabrication of the corrugated plate requires complicated procedures. To reduce the contact area between separator components and electrolyte, the separator plate's design should be modified and simplified. The press stamping method leads to cost reductions in production, and changing the mould base pattern leads to a better shape of the separator to avoid electrolyte loss.

With this background information, Chubu Electric Power Company, MCFC producer IHI, and CRIEPI started studying the performance and life expectancy of 100 cm^2 scaled MCFC cells with a Li/Na carbonate electrolyte. The measured cell voltage of the Li/Na carbonate applied cells was higher than the voltage of the Li/K carbonate applied cells [14]. This result led us to carry out an operating test with a 10 kW-class stack using a Li/Na carbonate electrolyte to improve the MCFCs electricity generating performance. For this paper, 0.44 m^2/14 cell and 1.03 m^2/10 cell/10 kW-class stacks were applied in the operating tests. The purpose of using a 0.44 m^2/10 kW-class stack was to perform the basic performance tests at an operating current density between 1500 and 3000 A/m^2. The 0.44 m^2/10 kW-class stack was also applied in a 10,000 h endurance test for, however, as stated later, the voltage degradation rate observed in the endurance test was insufficient for commercial applications. To improve the voltage degradation rate of the MCFC stack, a 1.03 m^2 stack was provided for a 10,000 h endurance test. The analysis of the anode outlet gas composition measured by using gas-chromatography and the temperature distribution in the stacks is discussed thoroughly in the following.

Table 1
Material and specifications of 0.44 m^2/10 kW- and 1.03 m^2/10 kW-class stack

Reactive area	0.44 m^2 × 14 cells (0.44 m^2 stack); 1.03 m^2 × 10 cells (1.03 m^2 stack)
Gas flow path length of reactive area	0.56 m
Centre plate	Ni201–SUS310S clad steel
Anode/current collector	Ni–AlCr alloy/Ni
Cathode/current collector	In situ NiO/SUS316L
Electrolyte/matrix	Li_2CO_3/Na_2CO_3 = 60/40%/$LiAlO_2$
Matrix thickness	0.9 mm (0.44 m^2 stack); 1.2 mm (1.03 m^2 stack)
Geometry of gas flow	Co-flow

2. Experiment

2.1. Stack structure

Materials and specifications of the 0.44 and 1.03 m^2 stack are listed in Table 1. The stacks are fabricated by Ishikawajima-Harima Heavy Industry (IHI) Co., Japan. Each cell of the 0.44 m^2 stack has a reactive area of 0.44 m^2 and consists of 14 cells, whereas the 1.03 m^2 stack has a reactive area of 1.03 m^2 and 10 cells. The press stamping method is applied to mould the separators, which is cost-effective when the separators are mass-produced. In Fig. 1, the schematic shape of a press stamping separator is compared with a corrugated plate-type separator, which was applied in former stacks. There is no corrugated plate in the press stamping separator. The contact area between the separator plate and the electrolyte of the press stamping separator is smaller than the contact area when using the corrugated type separator; the shape is designed to diminish electrolyte loss. The material of the centre plate is Ni201–SUS310S clad steel; the anode is made of Ni–AlCr alloy, and the cathode of in situ oxidised Ni. Ni and SUS316L are added to the current collector of the anode and the cathode, respectively. The Li/Na ratio of the carbonate mixture is 60/40 mol%. The melting temperature of the carbonate mixture is around 500 °C; the melted carbonate mixture is supported by a $LiAlO_2$ matrix with a pore structure. According to investigations into the cathode current collector's material, significant corrosion caused by the Li_2/Na_2CO_3 carbonate around a temperature of 550 °C was detected on the SUS316L. To avoid corrosion of the current collector, steam has been added to the cathode gas at approximately 550 °C, which has the effect of avoiding corrosion caused by the Li_2/Na_2CO_3 carbonate.

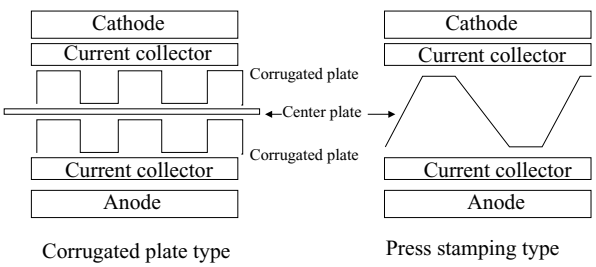

Fig. 1. Conceptual design of press stamping separator compared with corrugated plate-type separator.

To achieve a high current density operation, a greater amount of cathode gas should be supplied to keep the maximum temperature of the stack below 660 °C, as the corrosion of stack components increases drastically as soon as the stack temperature rises above 660 °C. The co-flow geometry is effective in removing heat out of the stack, because the temperature difference between gas inlet and outlet is large [15]. To be able to make a precise comparison of life expectancies, the gas flow geometry of 1.03 and 0.44 m^2 stacks were equalised.

2.2. Experimental equipment

Schematic pipelines and test stand equipment of the 0.44 m^2-class stack are presented in Fig. 2. The specifications of the test stand are listed in Table 2. The maximum operating pressure of the test stand is 0.7 MPa; the maximum operating temperature is around 700 °C; the maximum current density is more than 3000 A/m^2. The supplied fuel gas to the 10 kW-class stacks is a simulated reformed natural gas, which is a mixture of pure H_2, CO_2 and steam. The cathode gas is mixed with air and carbon dioxide; steam can also be supplied to the cathode. The cathode outlet gas in the 0.44 m^2 stack is re-circulated to the cathode inlet, as it is important to supply a great amount of cathode gas when operating under high current density conditions. To protect the cathode gas recycling blower from high temperatures and to cool down the exhausted cathode gas, the cathode outlet gas is cooled by a gas/water heat exchanger. Nitrogen is supplied to the pressure vessel, and the pressure difference between the cathode/vessel and anode/vessel are controlled. The 1.03 m^2 stack was operated in a different test stand, which had no gas re-circulation of the anode and cathode gas. Other than the gas re-circulation pipeline,

Table 2
Specifications of test stand

Operating condition	Capacity
Operating current	0 (OCV) ∼ 2400 A (for 0.44 m^2 stack); 0 (OCV) ∼ 3200 A (for 1.03 m^2 stack)
Operating pressure	Atmospheric pressure ∼ 0.7 MPa
Stack temperature	<700 °C
Supplied gas temperature	<700 °C
Pressure difference	Cathode and anode versus pressure vessel < 1000 mm H_2O (10 kPa)
Supplied gas condition	Pure H_2 ∼ simulated reformed natural gas ∼ coal gas ∼ CO
Recirculation of anode gas/cathode gas	Recirculating/recirculating (0.44 m^2 stack); single path/single path (1.03 m^2 stack)
Electrical output	10 kW (normal); 25 kW (maximum)

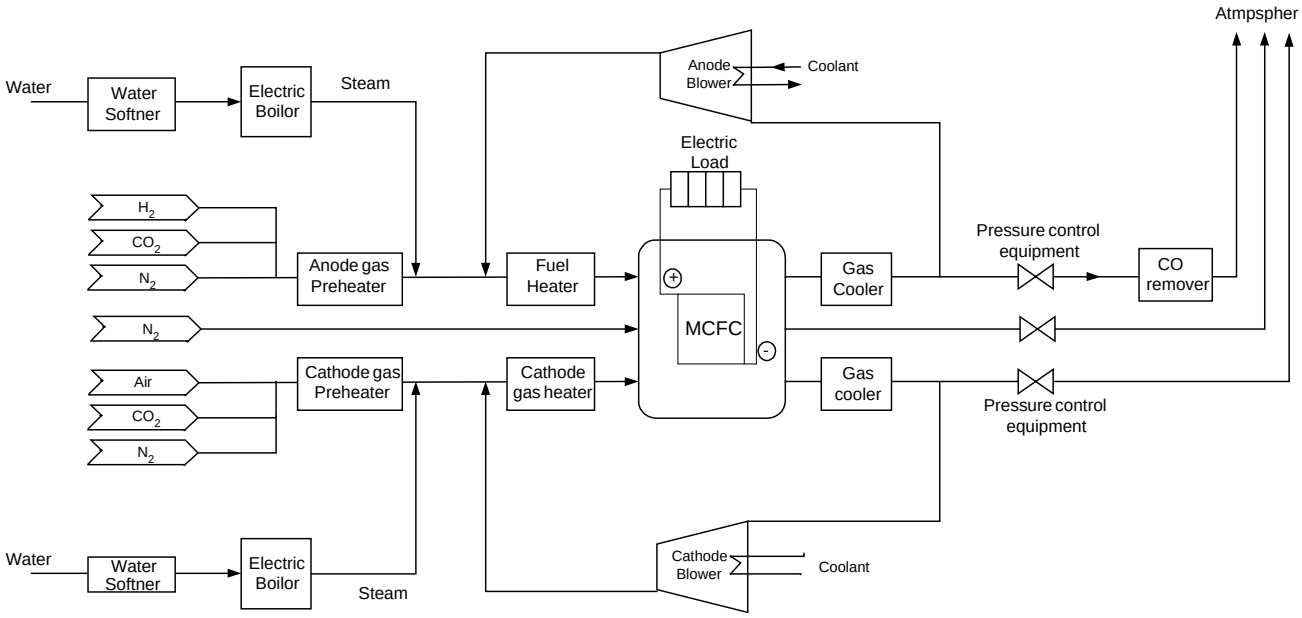

Fig. 2. Schematic pipeline and equipment of 0.44 m^2/10 kW-class stack test stand 1.03 m^2/10 kW-stack was operated in a different test stand with no recirculation of anode and cathode gas.

the specifications apply to the test stands of the 0.44 and 1.03 m^2 stacks.

The purpose of the 0.44 m^2/10 kW- and 1.03 m^2/10 kW-class stacks are summarised in Table 3. The 0.44 m^2 stack was operated from June 1998 to August 1999, and the 1.03 m^2 stack was tested from April 2001 to July 2002. After installing the stacks, each stack was operated for 10,000 h excluding the time required for test stand maintenance work.

2.3. Analysis method to estimate stack performance

Prior to the stack operating tests, a 100 cm^2 bench scale cell with the same reactive components as the 10 kW-class stack was used for experiments. The installation procedure of the bench scale cell corresponds with that of the 10 kW-class stack. In the cell test, the gas composition of the supplied gas, the operating pressure and operating temperature were changed; the current–voltage relation was derived according to the functions of the reactive gas partial pressure, the molar fraction of gases, and the cell temperature [16].

The relation between cell voltage and current density is written as follows:

$$V \cong E - (R_{ir} + R_a + R_c)\, j \tag{1}$$

V and E are cell voltage and Nernst voltage, respectively, R_{ir}, R_a, R_c, R_p represent the cell resistance, and j refers to the current density of a single cell. The Nernst voltage and the cell resistance are regulated as follows:

$$E = E^0 + \frac{RT}{2F} \ln \frac{p_{H_2,a}\, p_{CO_2,c}\, p_{O_2,c}^{1/2}}{p_{CO_2,a}\, p_{H_2O}} \tag{2}$$

Here, E^0, R, T, F and p_i describe the standard electromotive force, universal gas constant, cell temperature, Faraday's constant, and partial pressure of the gas composition i (subscript a and c refer to anode and cathode), respectively. The internal resistance and the anode and cathode reaction resistance are expressed as follows:

$$R_{ir} = A_{ir} \exp\left(-\frac{\Delta H_{ir}}{RT}\right) \tag{3}$$

$$R_a = A_a T \exp\left(-\frac{\Delta H_a}{RT}\right) P_{H_2,a}^{-0.5} \tag{4}$$

Table 3
Purpose of 0.44 m^2/10 kW- and 1.03 m^2/10 kW-class stack

	0.44 m^2/10 kW-class stack	1.03 m^2/10 kW-class stack
Purpose of initial test	Estimation of Li/Na electrolyte stack performance; high current density	Confirmation of basic stack performance
Purpose of endurance test	To evaluate stability of Li/Na electrolyte and press stamping separator	To improve voltage degradation rate of Li/Na electrolyte and press stamping separator

Table 4
Coefficients and activation energy of cell

Parameters	Magnitude
A_{ir} ($\Omega\,cm^2$)	1.38E−2
ΔH_{ir} (J/mol)	23.8E3
A_a ($\Omega\,cm^2\,atm^{0.5}\,K^{-1}$)	9.5E−7
ΔH_a (J/mol)	27.9E3
A_{c_1} ($\Omega\,cm^2\,atm^{0.25}\,K^{-1}$)	6.91E−15
ΔH_{c_1} (J/mol)	179.2E3
A_{c_2} ($\Omega\,cm^2\,K^{-1}$)	3.75E−9
ΔH_{c_2} (J/mol)	67.2E3
A_{c_3} ($\Omega\,cm^2$)	1.07E−6
ΔH_{c_3} (J/mol)	95.2E3

$$R_c = A_{c_1} T \exp\left(-\frac{\Delta H_{c_1}}{RT}\right) P_{O_2,c}^{-0.75} P_{CO_2,c}^{0.5} + A_{c_2} T \exp\left(\frac{\Delta H_{c_2}}{RT}\right) \times \left\{ m_{CO_2,c} + A_{c_3} m_{H_2O,c} \exp\left(\frac{\Delta H_{c_3}}{RT}\right)\right\}^{-1} \quad (5)$$

m_i designates the partial pressure and the mole fraction of the chemical species i, A_{ir}, A_a, A_{c_1}, A_{c_2}, A_{c_3} refer to the coefficient of the internal resistance and the anode and cathode reaction resistance, ΔH_{ir}, ΔH_a, ΔH_{c_1}, ΔH_{c_2}, ΔH_{c_3} give an indication of the activation energy, respectively. These coefficients and values of activation energies are derived from tests on bench scale cells, which have a reactive area of 100 cm^2. Every parameter appearing in these equations is listed in Table 4. By applying the cell performance equation, it is possible to calculate the electrical output and the current density distribution in the stack.

3. Basic performance of the Li/Na MCFC stack

3.1. Performance analysis of the 0.44 m^2/10 kW-class stack

The cell voltage dependency on the fuel utilisation of the 0.44 m^2 stack is compared with the calculated cell voltage in Fig. 3. The supplied fuel is a 30% humidified simulated natural gas with a $H_2/CO_2/H_2O$ ratio of 56/14/30. The 70% air and 30% CO_2 mixed gas is supplied from outside the cathode re-circulation loop, and around 70% of the cathode outlet gas is re-circulated to the cathode inlet. The operating current density and the pressure are set at 1500 A/m^2 and 0.49 MPa, respectively. The anode/cathode gas inlet temperature at the gas header is maintained at 605/600 °C. During the evaluation procedure of the calculated cell voltage, the stack components are divided into 20 control volumes in gas flow direction, and the current–voltage relation in each control volume is estimated according to Eq. (1) and the parameters in Table 4. There is an assumption that the individual cell voltages do not apply to other cells in gas flow direction; whereas the temperature and the current density also apply to other cells in gas flow and stacking direction.

The differences between the cell voltages are within 10 mV except for cell no. 14, which is located at the bottom of the stack. The cell voltage gradient of cell no. 14 is a gentle slope compared to the other cells, and this fact suggests that a lot of fuel gas flowed into cell no. 14. There is a reasonable correspondence between the calculated cell voltage and the measured cell voltage. The correspondence signifies that the installing procedure of the bench scale cell is also suitable for the 10 kW-class stack. It also allows us to estimate the thermal efficiency of the MCFC plant by applying Eqs. (1)–(5) with the parameters and activation

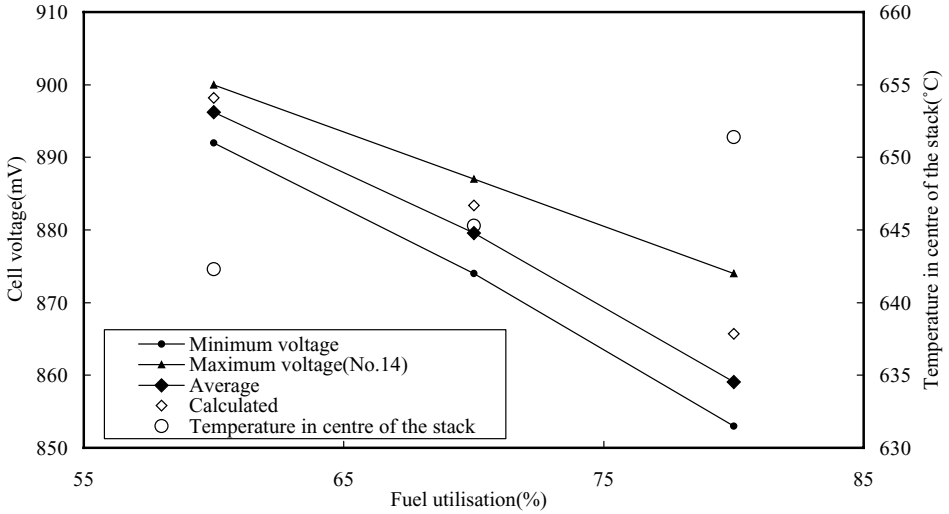

Fig. 3. Measured and calculated cell voltage with the measured temperature in stack centre versus set fuel utilisation, reactive area = 0.44 m^2, number of cells = 14 cells, operating pressure = 0.49 MPa, operating current density = 1500 A/m^2, $H_2/CO_2/H_2O$ of fuel gas = 56/14/30 (30% humidified simulated reformed natural gas), air/CO_2 ratio of cathode gas composition = 70/30, cathode gas re-circulating ratio = 65%.

energy listed in Table 4. In Fig. 3, the separator temperature in the centre of the stack is measured by a thermocouple and is plotted versus the fuel utilisation. The voltage drop is responsible for a greater heat evolution in the stack; the increased fuel utilisation also leads to a smaller fuel gas flow rate: The current density increases in the region of the fuel gas inlet due to the greater fuel utilisation. These three factors have an influence on the temperature distribution in the stack, the temperature in the centre of stack for example rises with the fuel utilisation as shown in Fig. 3.

3.2. Modification of temperature analysis model surrounding top and bottom separator

The authors have developed a numerical model to analyse the temperature distribution in the 100 kW-class MCFC stack [17]. Regarding the temperature analysis, the adiabatic heat flow in stacking direction is an assumption since the 100 kW-class stack consists of many cells (approximately 100 cells), and the stack's heat loss has a minor influence on the temperature distribution in stacking direction. In the temperature analysis of the 10 kW-class stack, however, the heat loss and the heat transfer, for which the stack holder is responsible, have an effect on the temperature distribution in the stack due to fewer cells. Without taking account of the heat loss and the heat transfer, the analysed temperature distribution differs greatly from the measured temperature distribution in the 10 kW-class stack. Researchers in ECN, The Netherlands, have estimated the heat transfer effect of the stack holder for internal reforming type MCFC stacks [18]. According to their results, the heat flows in the opposite direction to the gas along the stack holder, and the analysed temperature distribution including the heat effect of the stack holder agrees with the measured temperature. Our temperature analysis model has been expanded to take account of the area around the stack, and the heat transfer, for which the stack holder is responsible, has been introduced into the external reforming type MCFC stack. A schematic model of the analysis area of a 100 kW and a 10 kW-class stack is presented in Fig. 4.

Since the stack's heat loss to its surroundings has a great influence on the temperature of a 10 kW-class stack, the heat loss rate was measured during stack operation. A 0.44 m^2/10 kW-class stack in a pressure vessel was surrounded by heat insulating material, and two thermocouples were attached to both sides of the heat insulating material. According to the temperature difference on both sides of the thermal insulation, the heat flow rate was estimated at approximately 1.2 kW/m^2. This heat flow rate was applied to the temperature analysis of the 0.44 m^2/10 kW-class stack. To measure the temperature in the stack, thermocouples were inserted into the separator between cell no. 7 and no. 8. Further thermocouples were located at the bottom and the top of the separator. The thermocouples were fixed onto the reverse of the separator's reactive side. When testing the electrical output by means of connecting electric heaters to the stack holder, the only electric heater working was the one located on the gas inlet side. For this analysis, the thermal boundary condition was selected as described in Fig. 5. In Fig. 6, the calculated temperature distribution is compared with the measured temperature in gas flow direction and stacking direction. In the comparison, the centre of the gas flow width was selected as the position requiring discussion. A good agreement between the bottom of the anode and the top of the cathode separator was observed. Based on these results, the analysis model of the stack holder is required for the temperature analysis of the 10 kW-class

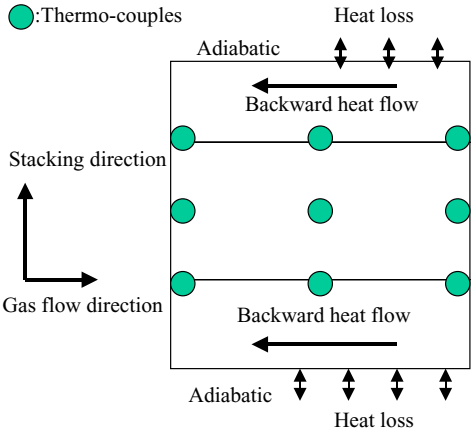

Fig. 5. Location of thermocouples and scheme of heat loss.

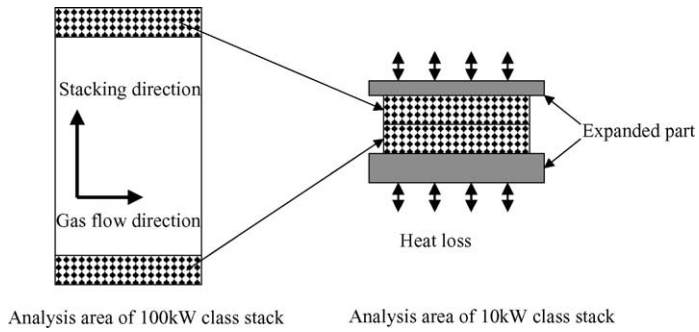

Fig. 4. Analysis area of 100 and 10 kW-class stack.

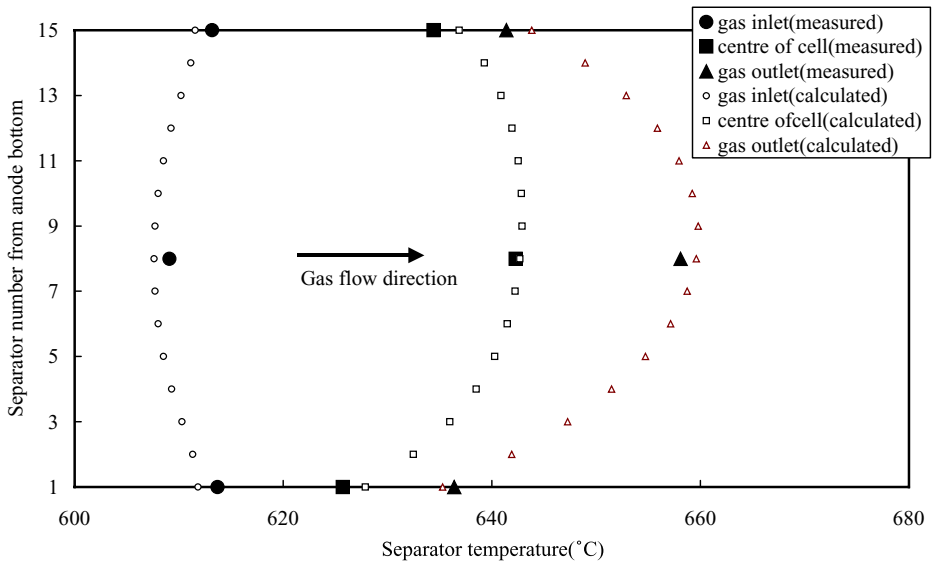

Fig. 6. Measured and calculated separator temperature, operating pressure = 0.49 MPa, current density = 1500 A/m^2, fuel gas composition (utilisation): $H_2/CO_2/H_2O$ = 56/14/30 (60%), cathode gas composition (CO_2/O_2 utilisation): air/CO_2 = 70/30 (30/30%), cathode gas re-circulating ratio = 65%, anode/cathode gas inlet temperature = 603/600 °C.

stack. This conclusion supports the basic idea of ECN, which states that the heat flow of the stack holder can also be applied to the external reforming type MCFC stack.

Our attention is focused on the temperature distribution of the stack under thermally isolated conditions, as the commercial stack does not have any electric heaters surrounding it, which would be a cost-effective method for the MCFC system. If a heat loss is supposed for each direction of the stack, the temperature distribution in thermally isolated conditions can be simulated. In Fig. 7, the temperature distribution is plotted for a heat loss of 1.2 kW/m^2 in each direction of the stack. The temperature of the bottom and the top separator is lower, however, the temperature maintains an operateable level because the heat transfer effect, for which the stack holder is responsible, compensates for the temperature at the gas inlet. According to this result, the stack can be operated with no electrical heaters in the practical stack with an operating current density of 1500 A/m^2.

3.3. High current density operation

The stack operating tests under high current density conditions were carried out using a 0.44 m^2 stack. Under high current density operating conditions, the stack requires a greater amount of cathode gas to maintain an adequate temperature level, i.e. 600–660 °C. A greater amount of cathode

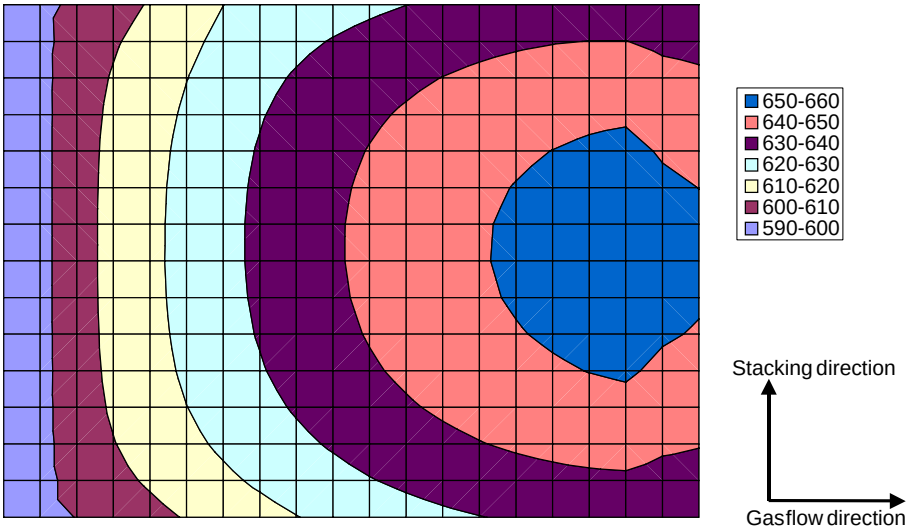

Fig. 7. Temperature distribution of MCFC stack operated in thermally isolated condition, calculated condition corresponds with Fig. 6 except for heat loss.

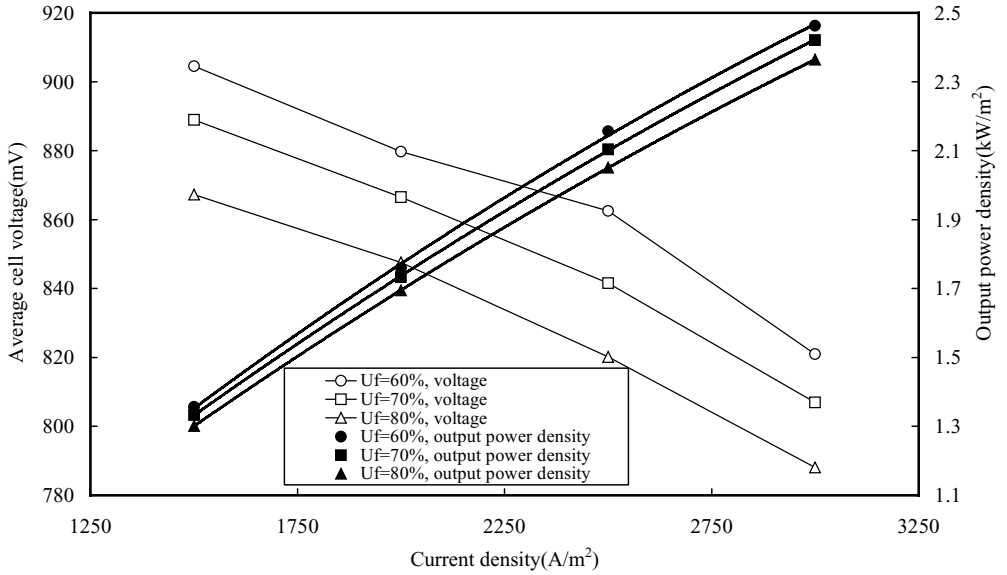

Fig. 8. Voltage and electrical output power density of 0.44 m^2/10 kW-class stack in high current density operating conditions, operating pressure = 0.69 MPa, $H_2/CO_2/H_2O$ ratio of fuel gas = 56/14/30, air/CO_2 ratio of cathode gas = 70/30.

gas causes the pressure drop along the cathode gas channel, which is responsible for a greater pressure difference between the cathode gas and the pressure vessel. The MCFCs gas channel is separated from the surrounding gas by the wetability of the carbonate melt. To avoid a leakage of cathode gas to the surroundings, the pressure difference should be kept lower than about 3 kPa. For the purpose of keeping the pressure difference at a lower level, the tests were carried out at high pressure, 0.69 MPa, since the pressure drop in the gas channel is lower under high operating pressure.

The current density was changed from 1500 to 3000 A/m^2 with a variation of fuel utilisations. The supplied fuel was a 30% humidified simulated natural gas. The 30% CO_2 and 70% air were added to the cathode gas and the exhausted cathode gas was re-circulated to the cathode inlet. In Fig. 8, the average cell voltage of the stack is plotted versus the operating current density with the parameters of the fuel utilisation. The maximum output power density of a 2.46 kW/m^2 was recorded at a current density of 3000 A/m^2 and a fuel utilisation of 60%. All cell voltages remained at more than 750 mV with a current density of 3000 A/m^2 independent of the fuel utilisation; the maximum temperature of the stack was lower than 665 °C. The measured voltage of the stack remained stable during the 2 weeks of the high current density

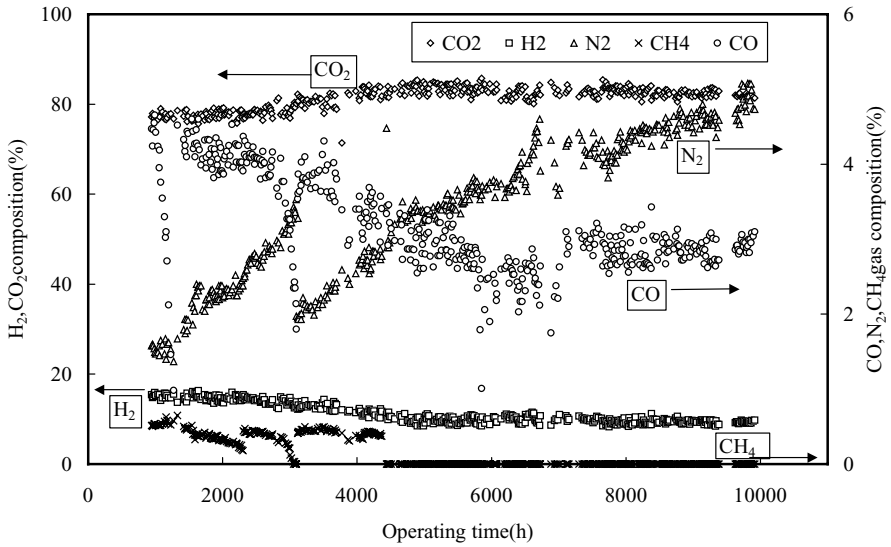

Fig. 9. Result of gas composition analysis using gas-chromatography, operating pressure = 0.49 MPa, current density = 1500 A/m^2, fuel gas composition (utilisation): $H_2/CO_2/H_2O$ = 56/14/30 (75%), cathode gas composition (CO_2/O_2 utilisation): air/CO_2 = 80/20 (51/30%), cathode gas re-circulating ratio ≒ 70%, anode/cathode gas inlet temperature = 590/580 °C.

operating test. The high current density test was also performed at an operating pressure of 0.49 MPa and the current density could be increased to 3000 A/m^2, however, it was not possible to set the fuel utilisation any higher than 60% because the maximum temperature rose significantly and the pressure drop of the cathode gas increased past the warning point.

4. Endurance test on Li/Na MCFC stack

4.1. Endurance test on 0.44 m^2/10 kW-class stack to evaluate stability of Li/Na stack

In Fig. 9, the anode outlet gas composition measured by the gas-chromatograph has been plotted versus the operating time. The focus was on the composition of the N_2 gas, however, a leakage was found between the anode and the pressure vessel at the beginning of the endurance test, and, therefore, the anode inlet gas pressure was controlled at 0.3 kPa lower than the pressure vessel to avoid a leakage of the anode gas to the surroundings. At an operating time of 3000 h, the anode inlet gas pressure was changed to create the same pressure as in the surroundings, because the leakage of the anode gas to the surroundings had increased. Watching the gas composition of CH_4 between 1000 and 4500 h, the measured composition of CH_4 dropped several times which was caused by the lack of the gas-chromatograph's accuracy. Between 4500 and 10,000 h, however, the gas composition of CH_4 was measured at zero without identifying any problems with the gas-chromatograph. The turning point was at an operating time of 4500 h, when the current density was changed to 0 A/m^2 (OCV) to measure the internal resistance.

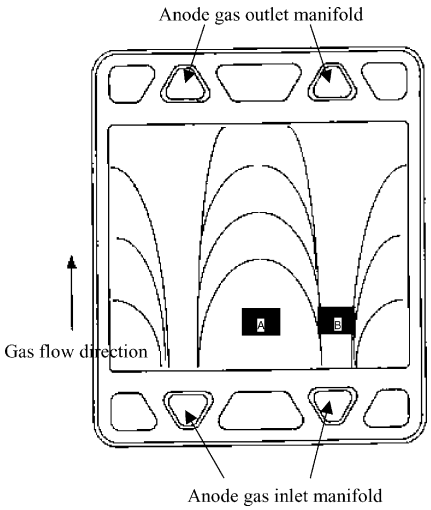

Fig. 11. Pattern of the crack on the surface of electrolyte matrix plate on anode side.

Between 2500 and 4500 h, the H_2 gas gradually decreased and the CO_2 gas increased. This fact suggests that Ni shortening occurred in the stack, because the same tendency was observed in the endurance tests of the bench scale cell (100 cm^2), which had had the same reactive components as the 0.44 m^2 stack. The shortening was unexpected Ni shortening, which seemed to be caused by the defective formation of the matrix. As soon as Ni shortening occurs, the fuel utilisation increases in comparison to the set value. In Fig. 10, the fuel utilisation calculated by the gas composition analysis of the anode outlet gas, i.e. observed fuel utilisation, is compared with the fuel utilisation set by the gas flow rate of H_2. Before an operating time of 2500 h, the observed fuel utilisation was around 75%, which was similar to the value

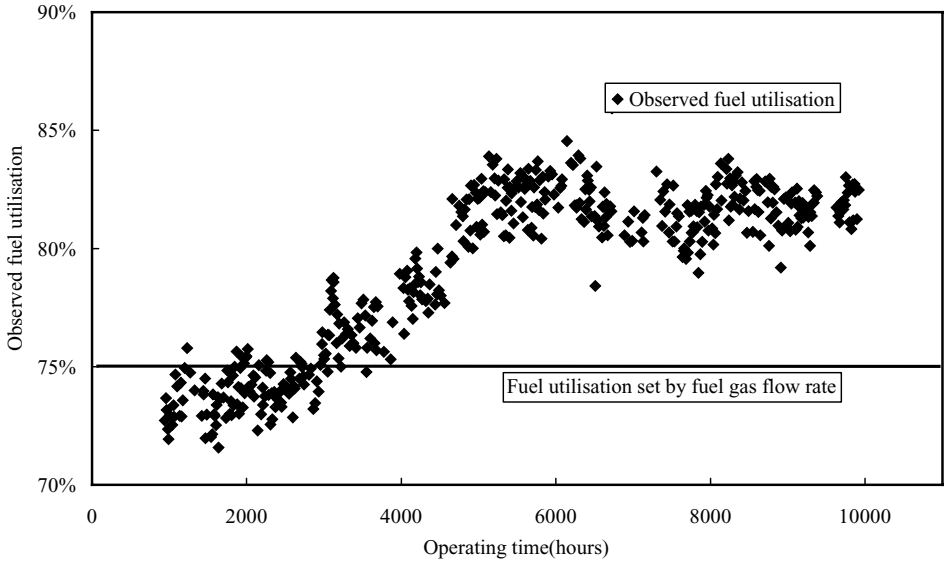

Fig. 10. Change of observed fuel utilisation versus operating time, set fuel utilisation is 75%, observed fuel utilisation is calculated from anode outlet gas composition measured by gas-chromatography.

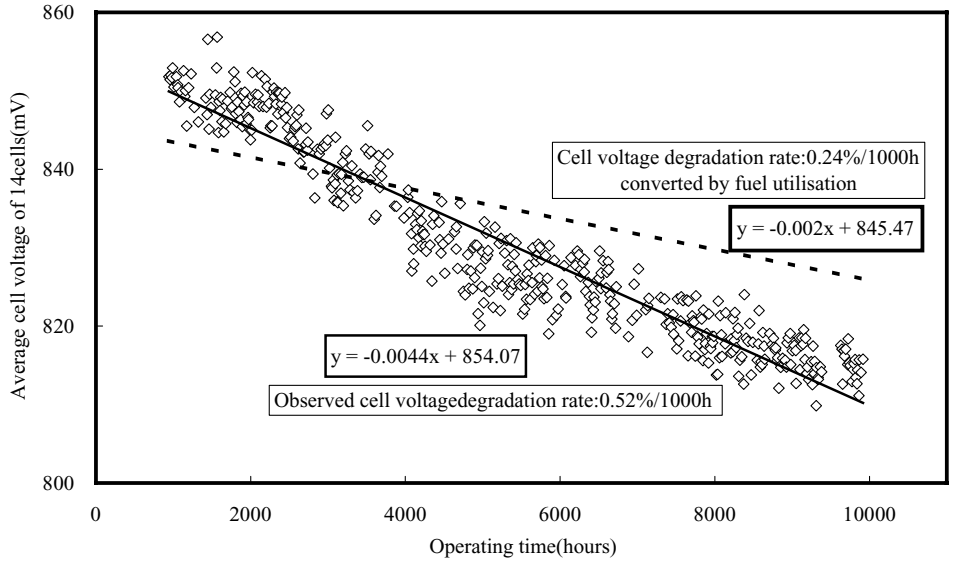

Fig. 12. Average cell voltage versus operating time, dotted line is converted cell voltage according to fuel utilisation. Operating pressure = 0.49 MPa, current density = 1500 A/m^2, fuel gas composition (utilisation) = $H_2/CO_2/H_2O$ = 56/14/30 (75%), cathode gas composition (CO_2/O_2 utilisation): air/CO_2 = 80/20 (51/30%), cathode gas re-circulating ratio ≒ 70%, anode/cathode gas inlet temperature = 590/580 °C.

set by the gas flow rate, however, between 2500 and 5000 h, the observed fuel utilisation increased due to shortening.

After the endurance test on the 0.44 m^2/10 kW-class stack, the stack was separated into individual cells to perform a post-test analysis. All cells were separated between the anode and the electrolyte matrix. Several cracks were identified on the surface of the electrolyte matrix showing traces of the anode gas flow. The pattern of the cracks is presented in Fig. 11. The positions of the anode gas manifolds are designated in the figure; the manifolds without designation are cathode gas manifolds. The cracks seem to have occurred from the beginning of the operating test. Ni particles can be observed along the cracks; they seem to have been the cause for the Ni shortening between 2500 and 4500 h. A short circuit path between the cathode and the anode could not be detected in the post-test, however, it seems highly probable that the Ni shortening along the cracks is caused by Ni shortening. In accordance with the endurance test and the post-test, the matrix should be modified to achieve a longer life expectancy of the 0.44 m^2/10 kW-class stacks.

If the matrix had been made of an appropriate material and if the right method had been applied, the shortening would not have occurred during the endurance test. To eliminate the voltage drop due to shortening, the average cell voltage of the stack was changed according to the observed fuel utilisation. In Fig. 12, the average cell voltage of 14 cells

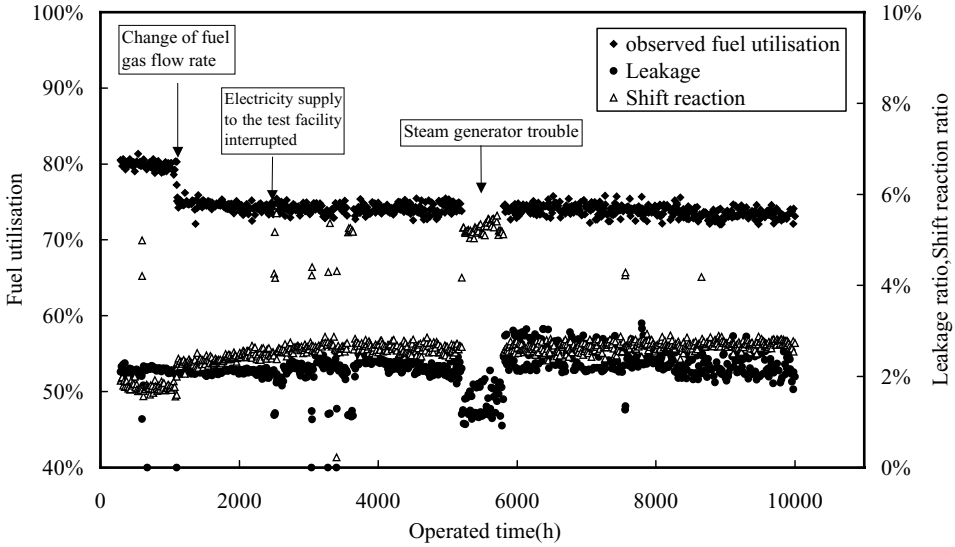

Fig. 13. Fuel utilisation, leakage ratio shift reaction rate calculated according to the measurement of anode outlet gas composition versus operating time.

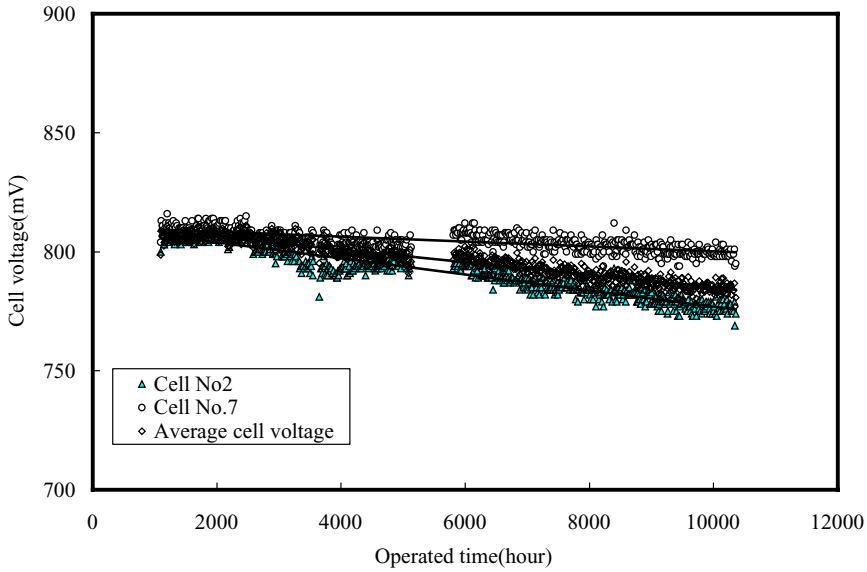

Fig. 14. Minimum, maximum and average cell voltage versus operating time, operating pressure = 0.49 MPa, current density = 1500 A/m^2, fuel gas composition (utilisation): $H_2/CO_2/H_2O$ = 56/14/30 (75%), cathode gas composition (CO_2/O_2 utilisation): air/CO_2 = 80/20 (51/30%), cathode gas recirculating ratio ≒ 70%, anode/cathode inlet gas temperature = 590/580 °C.

is mapped versus the stack operating time. The observed voltage decay rate is approximately 0.52% during 1000 h. The dotted line in Fig. 12 is the voltage changed according to the observed fuel utilisation. The degradation rate of the changed average cell voltage is approximately 0.24% over 1000 h. According to the result analysis, the 0.44 m^2 stack could operate at approximately 0.2–0.3% over 1000 h if the matrix were to be revised and the unexpected Ni shortening could be prevented. No other shortening was observed during the 10,000 h operation of the 0.44 m^2 stack.

4.2. Endurance test on 1.03 m^2/10 kW-class Li/Na MCFC stack to achieve low voltage degradation rate

For the purpose of estimating the cell voltage degradation rate in a MCFC stack, a 10 kW-class stack with a reactive area of 1.03 m^2 and 10 cells was installed into the test stand. The length of the gas flow path in the 1.03 m^2 stack corresponds with that in the 0.44 m^2 stack, whereas the width of the reactive area is 2.3 times longer than in the 0.44 m^2 stack.

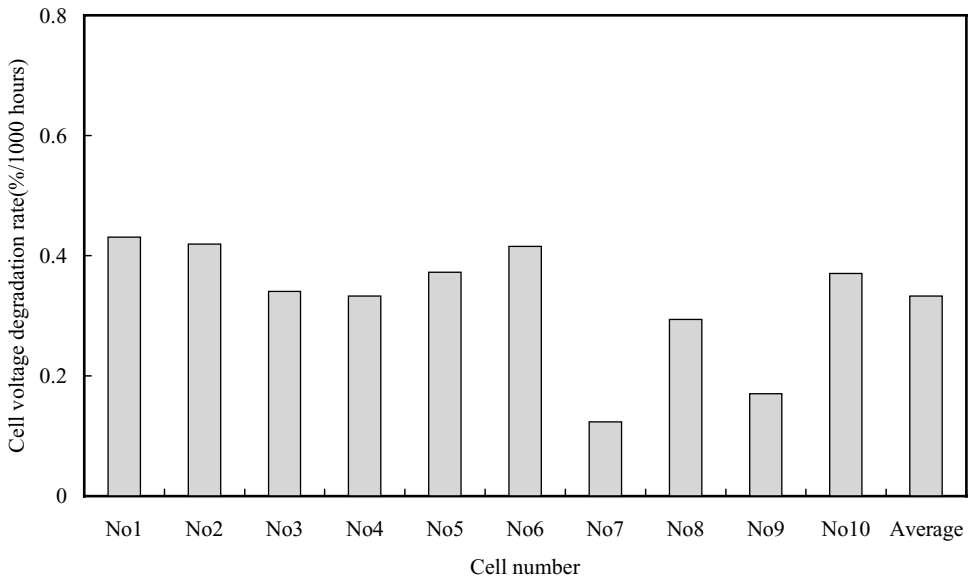

Fig. 15. Voltage degradation rate of each cell in 1.03 m^2/10 kW-class stack, operating pressure = 0.49 MPa, current density = 1500 A/m^2, fuel gas composition (utilisation): $H_2/CO_2/H_2O$ = 56/14/30 (75%), cathode gas composition(CO_2/O_2 utilisation): air/CO_2 = 90/10 (27/7%), 5% humidified, no cathode recirculation, anode/cathode inlet gas temperature = 590/580 °C.

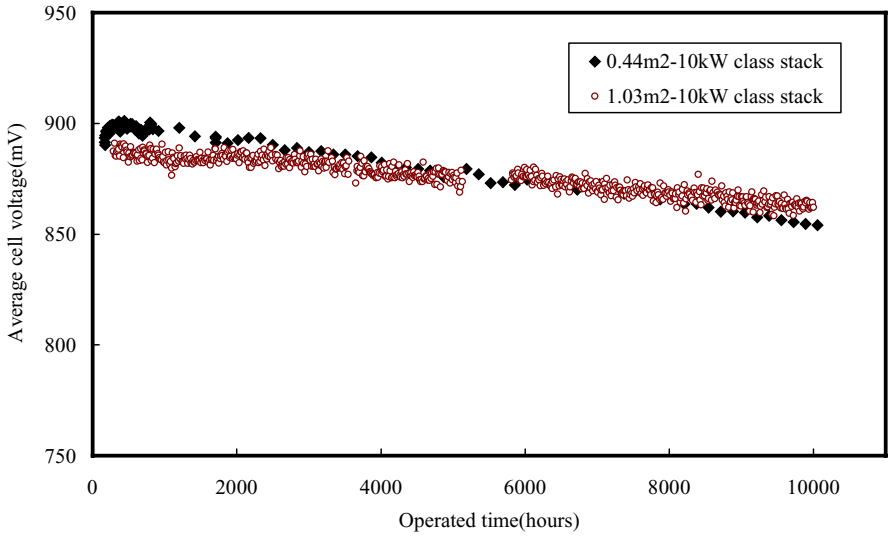

Fig. 16. Comparison of the average cell voltage of 0.44 m^2/10 kW- and 1.03 m^2/10 kW-class stack. Compared operating conditions: operating pressure = 0.49 MPa, current density = 1500 A/m^2, fuel gas composition (utilisation): $H_2/CO_2/H_2O$ = 56/14/30 (60%), cathode gas composition: air/CO_2 = 70/30.

Since the 0.44 m^2 stack was subject to Ni shortening, the matrix material of the 1.03 m^2 stack has been revised (detail not shown). The thickness of the matrix is 1.2 mm, whereas the matrix thickness of the 0.44 m^2/10 kW-class stack was 0.9 mm. In Fig. 13, the observed fuel utilisation has been plotted in relation to the operating time of the 1.03 m^2 stack. Due to the inaccuracy of the fuel flow rate controller, the fuel utilisation exceeded 75% up until an operating time of 1000 h. Based on the gas composition analysis of the anode outlet gas up until the same time, the fuel flow rate was changed to 75%. At an operating time of approximately 2500 h, there was a power failure and the electricity supply to the test facility was interrupted for 2 h; the stack was totally out of control. The stack temperature decreased, however, the stack was able to maintain the melting temperature of carbonate. Between 5500 and 6000 h, the current density was changed to 250 A/m^2 because of the trouble with the steam generator.

Operating pressure, current density, fuel utilisation, fuel gas composition, cathode CO_2 utilisation and cathode gas composition were 0.49 MPa, 1500 A/m^2, 75%, $H_2/CO_2/H_2O$ = 56/14/30, 27%, and air/CO_2(+H_2O) = 90/10(+5), respectively. The fuel utilisation remained at 75% during the 10,000 h endurance test, which proves that no shortening occurred in the 1.03 m^2 stack. The shift reaction ratio and leakage ratio are displayed in the same figure. There was a leakage from the start of the endurance test, however, the leakage never increased in comparison to the leakage in the 0.44 m^2 stack. The shift reaction rate also maintained a constant value, and this fact proves that the electricity generating condition of the anode gas did not change during the 10,000 h endurance test.

In Fig. 14, the voltage of cell no. 2 and no. 7 are indicated together with the average cell voltage. Cell no. 2 and no. 7 had the lowest and highest voltage values. The calculated cell voltage was 812 mV, and this voltage agreed with the voltage of the 1.03 m^2 stack at the beginning of the endurance test. The cell voltage degradation rate of each cell is presented in Fig. 15. The degradation rate of the average cell voltage was around 0.3% over 1000 h, whereas the voltage degradation rate of a 0.44 m^2 stack is around 0.5% over 1000 h. This improvement of the voltage degradation rate was due to the revision of the matrix. As seen in Fig. 16, the performance of the 1.03 m^2 stack exceeded the performance of the 0.44 m^2 stack during the 10,000 h operation due to the improvement of the voltage degradation rate by 0.3% over 1000 h.

5. Conclusion

A 10 kW-class MCFC stack has been developed which applies a Li/Na carbonate electrolyte with a press stamping separator. According to the results of the stack operating tests and the calculation of the temperature distribution within the stack, the following can be concluded:

(1) The fuel utilisation dependence of the calculated cell voltage agrees with the fuel utilisation of the measured average cell voltage in the stack. This result allows us to estimate the MCFC performance in a commercial power plant by applying Eqs. (1)–(5) with the parameters and activation energy listed in Table 4.
(2) The calculated temperature distribution agrees with the measured temperature whilst taking account of the heat transfer of the stack holder. This result corresponds with those of the researchers in ECN for internal reforming MCFC stacks. The temperature of the cells located at the top and the bottom of the stack maintain a operateable

value if the MCFC stack is operated under thermally isolated condition.

(3) The 2.46 kW/m^2 has been recorded at a current density of 3000 A/m^2 for a 0.44 m^2/10 kW-class stack, and a stable electricity generation has been identified under high current density operating conditions.

(4) Unexpected Ni shortening occurred in the 0.44 m^2/10 kW-class stack due to the defective formation of the electrolyte matrix. The shortening seems to have been caused by cracks in the electrolyte matrix. The voltage degradation rate of the 0.44 m^2/10 kW-class stack was insufficient for practical use.

(5) The matrix has been revised for the operating test on the 1.03 m^2/10 kW-class stack. The installation performance of the 1.03 m^2/10 kW-class stack was lower than that of the 0.44 m^2/10 kW-class stack because of the different matrixes. The performance of the 1.03 m^2 stack, however, exceeded the performance of the 0.44 m^2 stack during the 10,000 h operation due to the improvement of the voltage degradation rate by 0.3% over 1000 h.

Acknowledgements

The temperature analysis model of the stack holder was derived in the discussion with Dr. Kraaij, Dr. Rietveld, Dr. Dekker and Dr. Makkus in ECN, The Netherlands. The authors would like to thank them and Professor Kas Hemmes at Delft University, who provided the opportunity for discussions in ECN and at the Delft University of Technology. A part of this work was conducted in cooperation with NEDO (New Energy and Industrial Technology Development Organisation) and the MCFC Research Association (Technology Research Association for Molten Carbonate Fuel Cell Power Generation System) in the context of the New Sunshine Programme conducted by MITI (Ministry of International Trade and Industry), Japan.

References

[1] Y. Mugikura, K. Asano, Electr. Eng. Jpn. 138 (1) (2002).
[2] H. Morita, Y. Mugikura, Y. Izaki, T. Watanabe, T. Abe, J. Electrochem. Soc. 145 (1998) 1511–1517.
[3] Y. Izaki, T. Watanabe, Y. Mugikura, H. Kinoshita, E. Kouda, T. Abe, T. Matsuyama, T. Shimizu, S. Sato, IFCC Proceedings, February 1992, pp. 243–246.
[4] Y. Izaki, T. Watanabe, T. Abe, M. Tooi, T. Matsuyama, M. Hosaka, JSME B 61 (592) (1995) 4477.
[5] H. Yasue, K. Takatani, Proceedings of the Third IFCC, Japan, 1999, pp. 251–254.
[6] G.J. Janz, F. Saegusa, J. Electrochem. Soc. 110 (5) (1963) 452–456.
[7] G.H.J. Broers, H.J.J. Van Ballegoy, Proceedings of the Third International Symposium on Fuel Cells, 1969, 77 pp.
[8] P.G.P. Ang, A.F. Sammells, J. Electrochem. Soc. 127 (6) (1980) 1287–1294.
[9] K. Tanimoto, Y. Miyazaki, M. Yanagida, S. Tanase, T. Kojima, N. Ohtori, H. Okuyama, T. Kodama, J. Power Sour. 39 (1992) 285–297.
[10] G. Mamantov, J. Braunstein, Advances in Molten Salt Chemistry, Plenum Press, New York, 1981.
[11] D.G. Lovering, Molten Salt Technology, Plenum Press, New York, 1982.
[12] C. Sishtla, R. Donado, E. Ong, R. Remick, Carbonate Fuel Cell Technology IV, Electrochemical Society, PV 97-4 315, 1997.
[13] K. Ota, S. Mitsushima, S. Kato, S. Asano, H. Yoshitake, N. Kamiya, J. Electrochem. Soc. 139 (3) (March 1992).
[14] Y. Mugikura, F. Yoshiba, Y. Izaki, T. Watanabe, K. Takahashi, S. Takashima, T. Kahara, J. Power Sour. 75 (1998) 108–115.
[15] H. Morita, M. Komoda, Y. Mugikura, Y. Izaki, T. Watanabe, Y. Masuda, T. Matsuyama, J. Power Sour. 112 (2002) 509–518.
[16] F. Yoshiba, N. Ono, Y. Izaki, T. Watanabe, T. Abe, J. Power Sour. 71 (1998) 328–336.
[17] F. Yoshiba, T. Abe, T. Watanabe, J. Power Sour. 87 (2000) 21–27.
[18] Kraaij, Rietvelt, Dekker, Mukkas, ECN, Private communication, January 6, 1999.